International Journal of Biological Macromolecules 292 (2025) 139098

Contents lists available at ScienceDirect

International Journal of Biological Macromolecules

journal homepage: www.elsevier.com/locate/ijbiomac

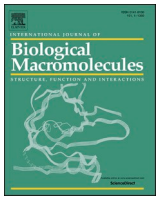

Unveiling the self-assembly process of gellan-chitosan complexes through a combination of atomistic simulations and experiments

Leonardo Severini [a,b,c,*,1], Letizia Tavagnacco [b,c,1], Simona Sennato [b,c], Erika Celi [d], Ester Chiessi [a], Claudia Mazzuca [a], Emanuela Zaccarelli [b,c,*]

[a] Department of Chemical Science and Technologies, University of Rome "Tor Vergata", Via della Ricerca Scientifica 1, 00133 Rome, Italy
[b] Institute for Complex Systems, National Research Council, Piazzale Aldo Moro 5, 00185 Rome, Italy
[c] Department of Physics, Sapienza University of Rome, Piazzale Aldo Moro 5, 00185 Rome, Italy
[d] CREA Research Centre for Olive, Fruit and Citrus Crops, Via di Fioranello 52, 00134 Rome, Italy

ARTICLE INFO

Keywords:
Polysaccharides
Polyelectrolyte complexes (PECs)
Self-assembly
Gellan gum
Chitosan
Fibers

ABSTRACT

Polyelectrolyte complexes (PECs), formed via the self-assembly of oppositely charged polysaccharides, are highly valued for their biocompatibility, biodegradability, and hydrophilicity, offering significant potential for biotechnological applications. However, the complex nature and lack of insight at a molecular level into polyelectrolytes conformation and aggregation often hinders the possibility of achieving an optimal control of PEC systems, limiting their practical applications. To address this problem, an in-depth investigation of PECs microscopic structural organization is required. In this work, for the first time, a hybrid approach that combines experimental techniques with atomistic molecular dynamics simulations is used to elucidate, at a molecular level, the mechanisms underlying the aggregation and structural organization of complexes formed by gellan and chitosan, i.e. PECs commonly used in food technology. This combined analysis reveals a two-step complexation process: gellan initially self-assembles into a double-helix structure, subsequently surrounded and stabilized by chitosan via electrostatic interactions. Furthermore, these results show that complexation preserves the individual conformation and intrinsic functionality of both polyelectrolytes, thereby ensuring the efficacy of the PECs in biotechnological applications.

1. Introduction

Molecular self-assembly plays a crucial role in the design of increasingly complicated and organized structures. Spontaneous association of simple molecules is considered a potential mechanism for the formation of the first ancestral biological macromolecules. Polysaccharide aggregation represents one of the most important self-assembly processes, playing a role in the emergence of living organisms and macromolecules at different length scales, from plants and bacteria to biological membranes, as well as in the formation of a double-stranded helix of DNA, protein folding and amyloid fiber organization [1–4]. Nowadays, inspired by natural structures, self-assembly strategies are exploited in the fabrication of hierarchical nano- and micro-materials with specific properties, shapes and dimensions [5,6]. As a consequence, there is a growing interest in the elucidation of the microscopic mechanisms underlying the self-assembly process, both in biological and artificial systems, thus leveraging the knowledge acquired for developing and optimizing the potential applications.

Self-assembled structures such as polyelectrolyte complexes (PECs), gels and aerogels, colloidal particles and micelles have been largely investigated to exploit their properties in many fields [7–10], which span from drug delivery, wound healing, renewable energy and cultural heritage preservation [11–15]. In this context, many efforts have been devoted to the development of DNA-chitosan complexes for biomedical applications and gellan-chitosan ones for food industry applications [16–18], where the formation of structures with different morphology, size and stability over time can be obtained using easy and quick experimental protocols by controlling the interaction between the oppositely charged polysaccharides. Nowadays, PECs are still able to attract large attention for their complex phenomenology, arising from a fine balance between long-range electrostatic interactions and short-distance steric ones. However, this complexity strongly challenges the

* Corresponding authors at: Institute of Complex Systems, National Research Council, Piazzale Aldo Moro 5, 00185 Rome Italy
E-mail addresses: leonardo.severini@roma1.infn.it (L. Severini), emanuela.zaccarelli@cnr.it (E. Zaccarelli).
[1] These authors contributed equally.

https://doi.org/10.1016/j.ijbiomac.2024.139098
Received 6 August 2024; Received in revised form 12 November 2024; Accepted 20 December 2024
Available online 26 December 2024

full understanding and prediction of their behavior. Among PECs, this work is focused on gellan-chitosan ones.

Gellan is a water-soluble, biocompatible and negatively charged exopolysaccharide, secreted by the microorganism *Pseudomonas elodea*, with high molecular weight [19]. It is composed of tetrasaccharide repeating units, i.e., D-Glc(β1 → 4)D-GlcA(β1 → 4)D-Glc(β1 → 4)L-Rha (α1 → 3) [7]. The polysaccharide, secreted by the microorganism, includes a L-glyceril and an acetyl group linked to the same glucose residue. However, treatment with alkali can remove the acyl substituents [20], leaving a carboxyl group on glucuronic acid residue, with a p*Ka* value of about 3.5 [21]. Gellan is well known for its gelling, structuring and stabilizing properties in the food and pharmaceutical industries. Moreover, in its physical hydrogel and microgel forms, it is extensively used as cleaning tool for different surfaces, such as paper artwork ones. Chitosan, a positively charged polysaccharide, is a product of deacetylation of chitin, either by chemical or biological treatments, and it is composed by randomly distributed β(1 → 4) linked D-glucosamine (deacetylated unit) and *N*-acetyl-D-glucosamine (acetylated unit) [22,23]. The properties of chitosan in solution depend on its molecular weight, degree of deacetylation, pH and ionic strength. In particular, its p*Ka* value spans from 6.2 to 7.0 depending on degree of deacetylation [24]. Chitosan is widely used in the field of biomedicine and food industry due to its biocompatibility, biodegradability and strong antibacterial properties [25,26].

PECs formed by gellan and chitosan have been investigated varying the preparation conditions, as well the addition of crosslinking agents and of surfactants. Indeed, chitosan polymer alone, despite providing antimicrobial activity, is very unstable in acidic environment, but such instability can be overcome by complexing chitosan with gellan, which resists up to low pH values [27–29]. Moreover, chitosan degrades due to the enzymatic activity of lysozyme, chitosanase and chitin deacetylase. Also in this case, the complexation with gellan hinders the binding between enzymes and chitosan, thus preventing its degradation [30]. Therefore, chitosan provides antimicrobial activity to the resulting complexes, while gellan ensures their stability. Despite the practical relevance of this peculiar system, there has been limited attention devoted to understand the main features of gellan-chitosan PECs formation. In particular, there is still no understanding at a molecular level of the aggregation mechanism of these two polysaccharides, so that their organization and conformation within the complexes is still a matter of debate in literature [31,32].

To fill this gap, the purpose of the present work is to perform an extensive study aimed at unveiling the key mechanisms ruling the interactions between gellan and chitosan, from macroscopic down to molecular scales, and thus to understand the formation and organization of the PECs. To reach this knowledge, the present study crucially involves a combination of experimental measurements and atomistic molecular dynamics (MD) simulations. Indeed, the latter are needed to complement experimental techniques, which are able to provide a good PECs characterization, but do not offer a precise identification of the microscopic features characterizing the assembly of the differently charged polysaccharides within the complexes. To the best of our knowledge, this is the first time that an original combined simulation/experimental approach for gellan-chitosan PECs investigation is reported in the literature. The underlying hypothesis of the present work is that the formation of the complexes involves different aggregation steps, but the microscopic organization of the two polyelectrolytes still ensures that their individual conformations are not affected, in order to maintain their specific functionalities also within the PECs. This hypothesis will be examined in the following by means of several experimental techniques including Dynamic and Dielectrophoretic Light Scattering (DLS, DELS), Atomic Force Microscopy (AFM), Attenuated Total Reflection FTIR (ATR-FTIR) and Circular Dichroism (CD) spectroscopy, that are used to probe complexes formation. These are complemented by MD simulations, which exploit the gellan force field recently developed and validated by the authors [7], aiming to provide a detailed molecular understanding of the different steps taking place in the complexation mechanism and of the final conformation of the PECs as a whole and also separately of gellan and chitosan.

2. Experimental section

2.1. Reagents and materials

Gellan (KELCOGEL used in low acyl form "highly deacetylated": KELCOGEL LA; *CAS*: *71010-52-1; Lot: 9G6158A*; molecular weight: 2–3 × 10^5 Da) powder was purchased from CP Kelco (San Diego, CA, USA). The repeating unit is a tetramer of one β-D-glucose-(1 → 4), one β-D-glucuronic acid-(1 → 4), one β-D-glucose-(1 → 4), and one α-L-rhamnose-(1 → 3). KELCOGEL LA contains the following average ionic composition: Na^+: 6330 ppm; K^+: 46800 ppm; Ca^{2+}: 3660 ppm; and Mg^{2+}: 1140 ppm [33]. The absence of the acetyl groups, within gellan chains, was confirmed by the analysis of NMR data reported in L. Severini, et al. [34].

Low molecular weight chitosan from shrimp shells (deacetylation ≥75 %; *CAS: 9012-76-4; Lot: STBG5431V*; molecular weight: 2–4 × 10^4 Da) powder was purchased from Sigma-Aldrich (St. Louis, MO, USA). It is composed of randomly distributed β(1 → 4)-D-glucosamine (75 %) and *N*-acetyl-D-glucosamine (25 %) units. The viscosity (1 % w/v in 1 % acetic acid = 20–300 cps) is theoretically consistent with molecular weight, according to the manufacturer's information. According to the supplier, chitosan was obtained with purity higher than 99 %. The determination of deacetylation degree (DD) of chitosan was performed by means of ATR-FTIR spectroscopy (Fig. S1), according to a procedure reported elsewhere [35], and circular dichroism measurements, discussed in the main text (see below). Hydrochloric acid, sodium hydroxide, perchloric acid, sodium acetate were purchased from Sigma-Aldrich (St. Louis, MO, USA). All reagents were analytical grade and used without further purification. In all cases, bi-distilled water (Millipore, Billerica, MA, USA) was used in the preparation of solutions.

2.2. Methods

2.2.1. Preparation of gellan and chitosan stock solutions

Gellan solution was prepared by dissolving gellan powder in bi-distilled water, under stirring, with final concentration of 1 % w/v (14 mM in saccharide units). The resulting mixture was heated up to 80 °C until becoming transparent. Then the homogeneous solution was cooled, down to room temperature, under stirring. Chitosan solution with a final concentration of 1 % w/v (14 mM in saccharide units) was prepared by dissolving chitosan powder in 100 mM sodium acetate buffer (pH 3) under stirring at room temperature overnight. Resulting solutions were diluted, as desired, using bi-distilled water.

2.2.2. Preparation of PECs, gellan and chitosan suspensions

To prepare PECs, proper volumes of gellan and chitosan stock solutions were mixed, maintaining a constant total polysaccharide concentration of 1 % w/v (14 mM). Different gellan:chitosan mole ratios of saccharide units (R) have been explored and, for clarity, PECs have been denoted with N_X, where the X-subscript refers to the gellan molar

Table 1
Saccharide units mole ratio, category and name of the proposed samples.

Gellan:chitosan mole ratio (R)	Category	Sample name
0.0:1.0	Reference	Chitosan (N_0)
0.3:0.7	Non-stoichiometric (excess chitosan)	$N_{0.3}$
0.5:0.5	Stoichiometric	$N_{0.5}$
0.7:0.3	Non-stoichiometric (excess gellan)	$N_{0.7}$
1.0:0.0	Reference	Gellan (N_1)

fraction within the complex, as detailed in Table 1.

The pH value of the solutions was adjusted to 4.5 using 0.1 M HCl (or $HClO_4$ for CD experiments, see below) or 0.1 M NaOH, depending on the starting pH. The resulting ionic strength of the system is 0.05 M. The mixtures were left for 30 min at room temperature, under stirring, for complete PECs formation.

2.2.3. Dynamic and dielectrophoretic light scattering measurements

Dynamic light scattering (DLS) and dielectrophoretic light scattering (DELS) measurements for determination of size and ζ-potential, respectively, were performed by the Nano Zetasizer ZS90 instrument (Malvern Instrument, UK), equipped with a polarized monochromatic beam emitted by a solid-state laser (100 mW; $\lambda = 642$ nm) and a thermostated cell holder. For DLS measurements, scattered light is collected at an angle $\Theta = 173°$ which corresponds to a scattering vector $q = 0.018$ nm^{-1}. The autocorrelation functions have been first analyzed by cumulant method [36], to get the average hydrodynamic size ($2R_H$) and the polydispersity index (PDI) of the samples, since this is the most direct way for determination of the size. However, when PDI values are larger than 0.2–0.3, this analysis may not be significant because the size distribution could show more than one maximum. To ascertain this point, a volume-weighted NNLS algorithm has been used, in the framework of the Mie scattering theory dispersion to determine the whole size distribution [37]. For this analysis, the refractive index of PEC has been approximated with the one of polystyrene. DELS measurements for determination of ζ-potential of PEC have been performed by means of laser doppler microelectrophoresis technique implemented with the M3-Phase Analysis Light Scattering (PALS) for a sensitive detection of the Doppler shift [38]. The electrophoretic mobility μ of the diffusing objects is then converted into a ζ-potential using the Smoluchowski relation $\zeta = \mu\ \eta/\varepsilon$, where ε and η are the permittivity and the viscosity, respectively, of the solution. Before analysis, all samples were diluted to a final concentration of 0.1 % *w/v* using bi-distilled water. Temperature was fixed to 25 °C in all the measurements.

2.2.4. Atomic force microscopy (AFM) measurements

AFM measurements were performed in air at room temperature using a DIMENSION ICON instrument (Bruker AXS, Germany) equipped with a Nanoscope V controller and enclosed in an insulating box. Images were collected in tapping mode using high resolution rotated-tapping mode etched silicon probes (RTESP), with a nominal tip radius of 8 nm. The samples were prepared by depositing 20 μL of each suspension on freshly cleaved mica for 60 s, then gently rinsing with 1 mL of MilliQ and drying in air for 30 min. Gwyddion free software was used to correct images by eliminating background and levelling defects.

2.2.5. ATR-FTIR spectroscopy

FTIR spectra of freeze-dried samples were acquired with the ThermoScientific instrument (model iS50) (Thermo Scientific Inc., Madison WI, USA) in Attenuated Total Reflectance (ATR) mode using a single reflection diamond ATR cell. Spectra were recorded in the wavenumbers region from 4000 to 525 cm^{-1}, averaging over 32 scans with a resolution of 2 cm^{-1}. All experiments were carried out in triplicate, yielding consistent and reproducible results. Spectra were baselined where no absorbance peaks are present (1950 cm^{-1}). The baseline-corrected spectra were normalized to the highest band, the characteristic carbohydrate fingerprint at ~1000 cm^{-1}, so that the absorbance of the highest peak is equal to 1.0.

2.2.6. Circular dichroism (CD) spectroscopy

Circular dichroism spectroscopy (Jasco J-700, Jasco Co, Tokyo, Japan) was performed on samples with concentration of 0.1 % w/v using a quartz cuvette with an optical path of 0.1 cm. Four accumulations for each CD spectrum were recorded at 25 °C with a scanning speed of 20 nm/min in the far-UV range (260–190 nm). The averaged spectrum of the baseline was subtracted for all shown spectra. All the solutions were acidified using perchloric acid.

2.2.7. Molecular dynamics simulations

All-atom molecular dynamics simulations were performed on a dispersion of gellan and chitosan chains in aqueous solution to characterize the mechanism of polyelectrolyte complexation with the GROMACS software package (version 2018) [39,40]. A gellan chain is made of 4 repeating units which corresponds to 16 saccharide units, and it is end-capped by methoxy groups. Gellan is described using the newly developed force field [7]. Starting atomic coordinates for the repeating unit were taken from the reported X-ray diffraction structure of oriented fibers of the gellan potassium salt [41]. Chitosan is modelled in its deacetylated form using the CHARMM36 force field for carbohydrates. A chitosan chain is composed by 16 saccharide units end-capped by methoxy groups to maintain the same number used for gellan. Starting atomic coordinates for a chitosan tetramer were taken from the crystal structure of its anhydrous form [42]. Simulations were carried out at polysaccharide mass fraction of 3, 5 and 10 % with a gellan:chitosan mole ratio of 0.5:0.5. To carefully reproduce the experimental conditions and to take into account the effect of the ionic strength on the polyelectrolyte complexation, simulations were performed in an aqueous solution of sodium chloride 50 mM. Salt and water were described using the CHARMM36 [43] and TIP3P [44] force fields, respectively.

In each system, four energy-optimized gellan chains with deprotonated glucuronic acid units and four energy optimized chitosan chains with charged amine groups were first inserted in a cubic box and oriented to maximize their distance. Water molecules corresponding to the set concentration, and sodium and chloride counterions were then added. The system was energy-minimized and equilibrated at 298 K for 50 ns. Trajectory data were acquired in the NPT ensemble for 1 μs at 298 K with a sampling frequency of 1 frame every 5 ps. For statistical purposes, and as a reference, an additional simulation of a suspension of six chitosan chains in water at a concentration of 5 wt% was also carried out following the same procedure. Details of the simulation protocol are as in ref. 7.

3. Results and discussion

3.1. Gellan-chitosan PECs formation

PECs with different gellan amount have been prepared, varying the molar ratio between the saccharide units of the two polysaccharides, with the aim to explore the condition of excess chitosan, i.e. excess of positive charge, where chitosan antimicrobial activity is reported [25,26]. This can be achieved at an acidic pH value of 4.5, where most of the amino groups of chitosan chains hold their cationic character. The mechanism of action of chitosan as an antimicrobial is not fully understood and several factors involved in the formation of PEC may tune this property [45], including the overall charge of the complexes. For this reason, the ζ-potential of the PECs prepared at the different gellan molar ratios of saccharide units (R) has been measured. Results, shown in Fig. 1, evidence that electrostatic complexation between gellan and chitosan takes place thus forming aggregates with positive charge. The ζ-potential value for pure gellan polysaccharide is negative (−30.5 ± 1.5 mV), as expected, because at pH = 4.5 its carboxyl moieties are mainly found in the deprotonated form. A similar consideration on the ionization degree is applicable to pure chitosan. In this case, the ζ-potential value is positive (+45.5 ± 2.3 mV), as the pH of the suspension is lower than the p*Ka* value of the polysaccharide, which is in the range of 6.2 to 7.0 [21,46,47] and the amino groups presented on each chitosan monomer are protonated. It can be concluded that this pH condition is effective to impart opposite charges to the two polyelectrolytes and to obtain electrostatic complexes.

The observed positive ζ-potential values of PECs can be easily justified by considering the relatively low charge density of gellan (0.25 mol

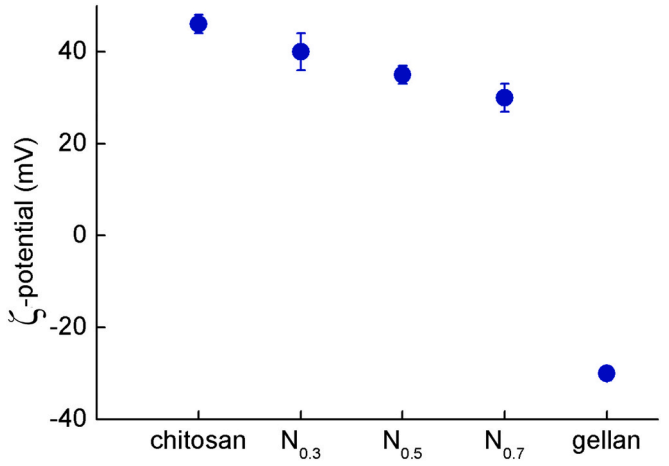

Fig. 1. ζ-potential values of chitosan, gellan and PECs at increasing gellan molar fraction N, as indicated in Table 1. Errors are the standard deviation of the mean value.

of negative charge/mol of saccharide units) [48] as compared to that of chitosan. In addition, other parameters, such as the charge distribution, the position of the ionic groups and the chain flexibility may affect the polyelectrolyte complexation [49]. The gellan:chitosan molar ratio R can be easily related to the stoichiometric charge ratio of the sample, defined by the ratio of the bare charges of the saccharide units, as usually defined in other investigations [50,51]. Since in the used experimental conditions the isoelectric charge ratio should be obtained at a molar fraction of about 0.8, the strongly positive values of the ζ-potential confirm the excess of chitosan charge, with respect to gellan, which is progressively reduced at increasing R. The ζ-potential value remains high for all PECs, thus indicating that the single gellan-chitosan complexes should be, on average, rather strongly charged and therefore have a good colloidal stability, because Coulomb repulsion is large enough to stabilize PECs and to avoid condensation.

The analysis of DLS data by the cumulant method showed the formation of heterogeneous aggregates with larger size compared to gellan and chitosan alone (data not shown). The increase in turbidity in $N_{0.3}$, $N_{0.5}$ and $N_{0.7}$ samples (Fig. S2) is clearly evident immediately after mixing, supporting the hypothesis of aggregate formation. DLS data are analyzed by volume-weighted NNLS algorithm (Fig. 2) and reveal the presence of different populations, as expected. Gellan shows a multimodal size distribution with a net prevalence of objects in the range 10–100 nm. In addition, it shows a weak peak around 500 nm probably associated to diffusion of larger structures formed by chain association [7]. Chitosan shows a bimodal size distribution, with the main peak occurring at a size around 6–7 nm [52,53], which corresponds to the contribution of single chains, considering that at this pH value aggregation is not expected. Several investigations have reported a polymer size ranging from a few to several tens of nanometers, depending on the ion concentration of the medium as well as on the persistence length and on the degree of acetylation of the employed chitosan [54]. The effect of the relative content R in gellan-chitosan mixtures is clearly visible by comparing the size distribution of the different PEC samples. The peaks related to the two polysaccharides alone cannot be any longer identified as such in any of the PEC samples, while structures spanning the whole size range from about ten to several hundreds of nanometers are observed. This suggests the existence of different types of complexes, which depend on the proportions between the two polysaccharides. Increasing gellan molar fraction up to 0.7, aggregates with a monomodal distribution with size around 200 nm are formed, suggesting the association in more homogenous structures. DLS and ζ-potential measurements were repeated one week after sample preparation, with comparable results, demonstrating a good stability of the systems over

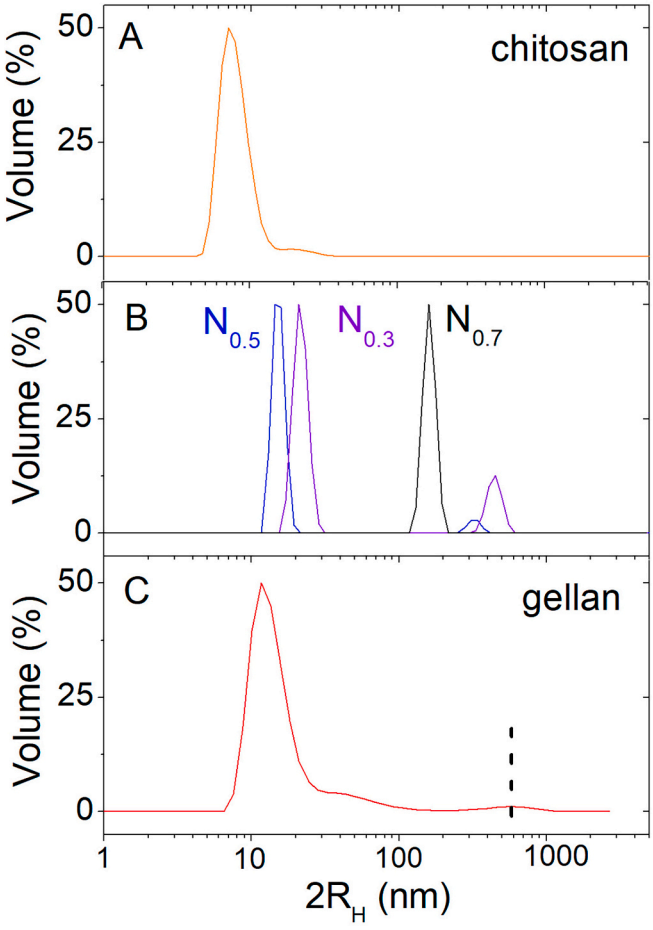

Fig. 2. Suspension characterizations for gellan, chitosan and PECs: volume-weighted size distribution of chitosan (A), PECs at different gellan molar fraction N (B) and gellan (C). The vertical dashed line in panel C marks the position of the peak attributable to association of gellan chains.

time.

An AFM investigation has been carried out to reveal the structure of each polymer dried on mica surface. Fig. 3 reports images of pure chitosan and gellan in panels A and B, respectively. Chitosan in acetate buffer at pH = 4.5 shows small nanostructures with spherical or elongated shape, and vertical size in the range 1–8 nm, with an average height of 1.5 ± 0.2 nm, as determined by grain analysis statistics on different images with a total of 50–70 objects. It should be noted that AFM measurements are performed with samples that are dried on a support, which causes flattening and deformation. This explains why the measured size is smaller than the one obtained by DLS on polymer solutions. The observed small globular structures are similar to those reported in literature for chitosan with deacetylation degree of 80.0 % ~ 95.0 %, dissolved in acetic acid at concentration lower than 0.05 mg/mL [55]. It is reported that polymer self-assembly on mica realizes a variety of objects ranging from globules to fibers and to more organized structures and thin films, whose formation depends on polymer concentration and many other factors which influence the hydrogen-bond network, such as pH, solvent, temperature, degree of acetylation, nature of salt and type of acids [56,57].

Fig. 3B shows the gellan hierarchical self-assembly of polymer into fibers, already observed in other investigations [58]. As expected on the basis of multimodal size distribution obtained by DLS, fibers of different lengths are present. The size of these fibers ranges from a minimum of 0.4 to a maximum of 3 nm, with an average value around 1 nm, which indicates the presence of chains with both primary and secondary

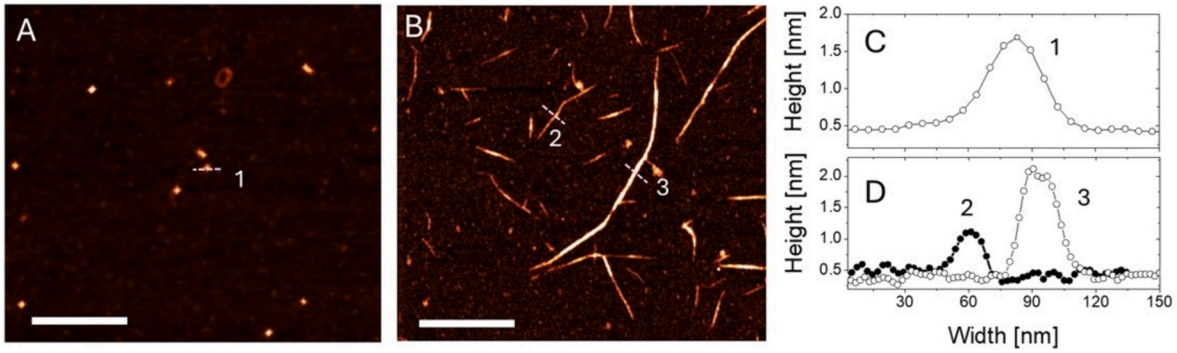

Fig. 3. AFM images (Height sensor) of chitosan (A) and gellan (B). The height profiles (C, D) and their corresponding sections on the images are labeled by matching numbers. Bar is 500 nm.

structures. The rigid fibrillar structure of the polymer can be inferred by the straight segments of the chain. The variation of the colour of the fiber along the longitudinal direction indicates an non-uniform thickness thus evidencing the lateral aggregation of multiple polymer chains.

Stoichiometric complexation of gellan and chitosan ($N_{0.5}$) gives rise to fibers of different length coexisting with other structures, as visible in Fig. 4A, and in the high magnification images (Figs. 4B, C, D). The small globular structures with a size of several nanometers (see the magenta rectangle, Fig. 4B, and the height profile, Fig. 4F), have the same features of pure chitosan (see Fig. 3A) and may be related to the presence of an excess of chitosan which remains free in suspension. The most interesting structures resulting from complexation are the fibers with evident bumps (Figs. 4C, D and corresponding height profile, Figs. 4E, G), regularly distributed on the longest fiber (Fig. 4D), as evidenced in the phase channel image (right side of Fig. 4D). These fibers are different from those observed in pure gellan (Fig. 3B) and the average height of their globular units is around 5 nm (Fig. 4E), larger than the one of the pure chitosan and gellan, thus suggesting polysaccharide aggregation.

3.2. Experimental evidence of gellan-chitosan mechanism of complexation

Chemical composition of the obtained suspensions has been investigated via Fourier transform infrared spectroscopy in ATR mode (ATR-FTIR). As shown in Fig. 5 spectra of gellan and chitosan alone display the characteristic carbohydrate fingerprint between 900 and 1200 cm^{-1} and a band at ~1430 cm^{-1} attributed to C–H bending vibrations [59,60]. Additionally, for gellan a band appears at ~1600 cm^{-1} [61], that is related to the presence of carboxylate moieties, while for chitosan a signal is present at ~1560 cm^{-1} [62], which is attributed to NH stretching. Expectedly, $N_{0.3}$, $N_{0.5}$ and $N_{0.7}$ mixed samples display all the characteristic bands of pure gellan and chitosan, indicating the successful incorporation of both components in the PECs. Increasing the

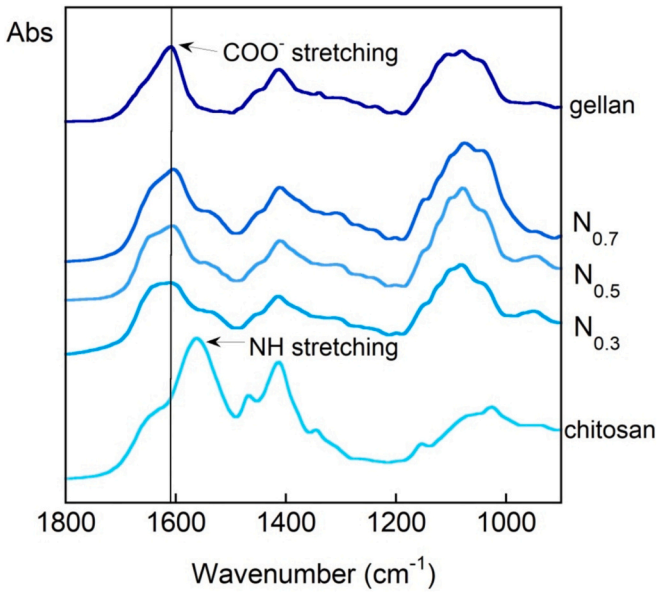

Fig. 5. Normalized absorbance ATR-FTIR spectra of chitosan, $N_{0.3}$, $N_{0.5}$, $N_{0.7}$ and gellan. Spectra are stacked for clarity. Characteristic peaks are indicated by arrows.

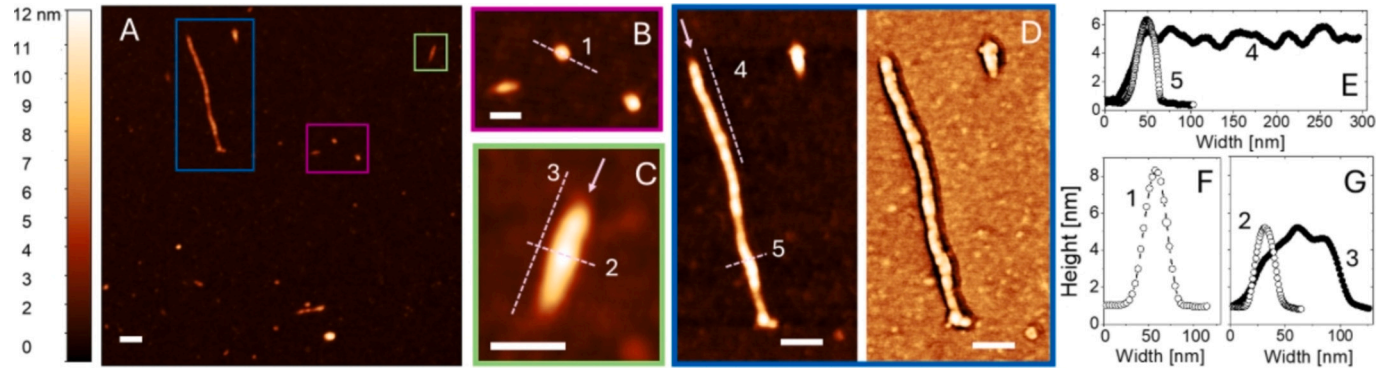

Fig. 4. AFM images (Height sensor) of PECs formed at gellan: (A) chitosan molar ratio $R = 0.5{:}0.5$ ($N_{0.5}$) and (B,C,D) high magnification images. Colour scale on the left refers to panel A, only. Panel D shows both the morphology by height sensor (left) and the phase channel image (right). The height profiles (panels E, F, G) and their corresponding sections on the images are labeled by matching numbers. Longitudinal sections following the direction of the arrow were shifted for clarity. Scale bar: 100 nm (panels A, D), 50 nm (panelsso B,C).

amount of gellan in the mixture, an enhancement of the intensity of the band attributable to carboxylate moieties is observed. Moreover, a slight shift towards lower wavenumbers (~1540 cm^{-1}) takes place for chitosan, due to the interaction with gellan. This last evidence is typical of symmetrical bending vibrations of amine salt in chitosan acid salt complexes [62].

Having confirmed the occurrence of aggregation between gellan and chitosan and the formation of PECs for all polysaccharides ratios described above, the subsequent investigation focused on the stoichiometric sample, $N_{0.5}$. For this sample, as well as for the corresponding pure gellan and pure chitosan samples, circular dichroism (CD) spectroscopy was exploited to obtain information regarding the conformation of the polysaccharides as such and in the polyelectrolyte complexes. Gellan coil to double-helix conformational transition is strongly pH- and temperature- dependent [63,64]. A decrease of pH, indeed, enhances the intermolecular aggregation of gellan chains. This is mainly due to the lower degree of ionization of carboxyl groups and therefore to the lower repulsion among gellan chains. Moreover, at temperatures below 30 °C the double-helix structure is favored. Herein, at the working temperature of 25 °C, this transition is highlighted by the change in ellipticity of the peak at ~200 nm, which is due to the carboxylate group in the repeating unit of gellan (Fig. S3). At a pH value of 6 a maximum is visible at 200 nm, attributable to the random-coil conformation of gellan. However, with decreasing pH up to 4.5, a minimum appears at 210 nm, which signals the presence of a double-helix structure (Fig. 6, Fig. S3). Chitosan CD spectrum, at the same pH and temperature conditions, shows a single peak at 210 nm, attributable to the chiral neighborhood of acetyl moieties. The intensity of this signal is dependent on the chitosan acetylation degree. As shown in Fig. 6, the recorded CD spectrum is consistent with that of a chitosan polymer with a degree of deacetylation ~75 %. Sample $N_{0.5}$ shows an experimental CD spectrum slightly different from the theoretical one (the latter calculated as the sum of the spectra of gellan alone and chitosan alone at the same concentration in the aggregate) at ~190 nm (Fig. 6). As reported in literature, in this high energy region, the amino groups of chitosan in the NH_2 form present a negative band [65]; the difference found in the PEC spectrum could therefore suggest an electrostatic interaction between the amino groups of chitosan and the carboxyl ones of gellan, confirming FTIR results. Moreover, this evidence also suggests that the interaction between the two polysaccharides does not affect gellan conformational features. The CD measurements were repeated in different days after sample preparation, finding similar results. This provides additional evidence of the stability of these complexes over time.

3.3. Formation mechanism of gellan-chitosan polyelectrolyte complexes from atomistic simulations

To gain a molecular understanding of the complexation mechanism of gellan and chitosan, complementary to the experimental approaches, atomistic molecular dynamics simulations of a suspension of polysaccharides with a gellan:chitosan stoichiometric molar ratio R = 0.5:0.5 ($N_{0.5}$) have been performed at ambient temperature (298 K).

The experimental conditions of pH have been carefully considered by modelling both gellan carboxylic groups and chitosan amine groups in the ionized state, as discussed in the section gellan-chitosan PECs formation. Simulations were carried out at a total polysaccharide mass fraction of 3, 5 and 10 % wt, which is a higher value than the one used in the experiments. This setup has been chosen to balance the size limitations of the in silico model associated to an atomistic representation and thus to allow the investigation of a significant ensemble of molecular species within a sustainable computing time. To properly account the effect of the ionic strength on the polyelectrolyte complexes formation, simulations were performed in an aqueous solution of sodium chloride 0.05 M, consistently with the salt content of the experimental sample.

Figs. 7A, B, C show some representative configurations of the polysaccharide chains suspensions at the different concentrations explored. All the systems reveal a clear tendency to self-assemble, which is more pronounced at the highest polysaccharide concentration of 10 wt%. In

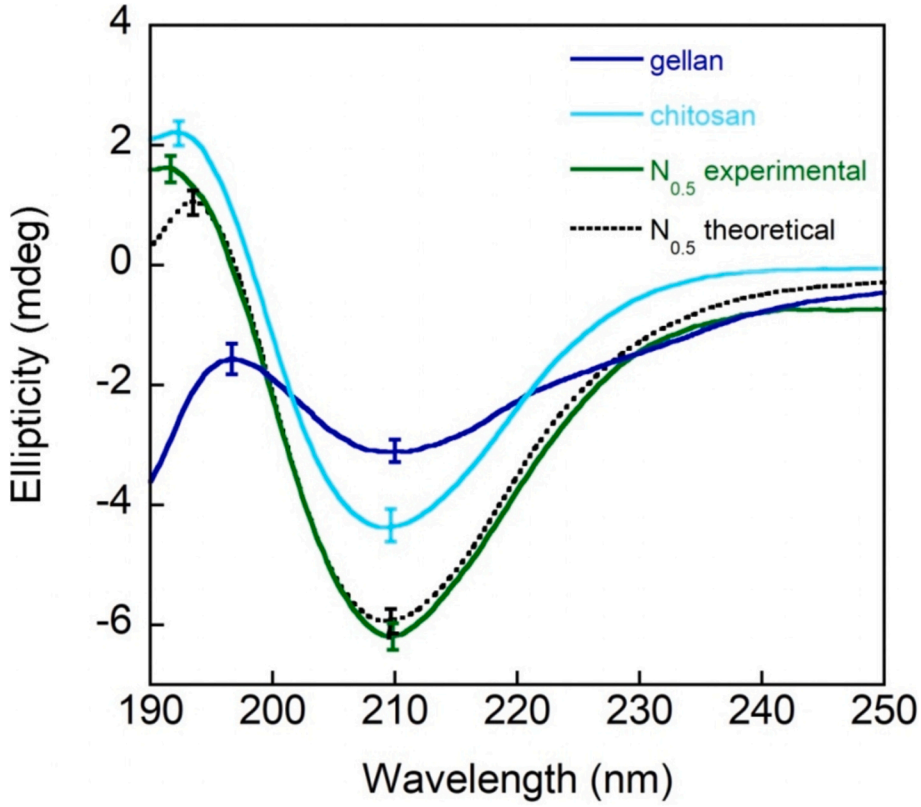

Fig. 6. Baseline subtracted CD spectra of chitosan, gellan and $N_{0.5}$ (experimental and theoretical) at T = 25 °C. Errors are the standard deviation of the mean value.

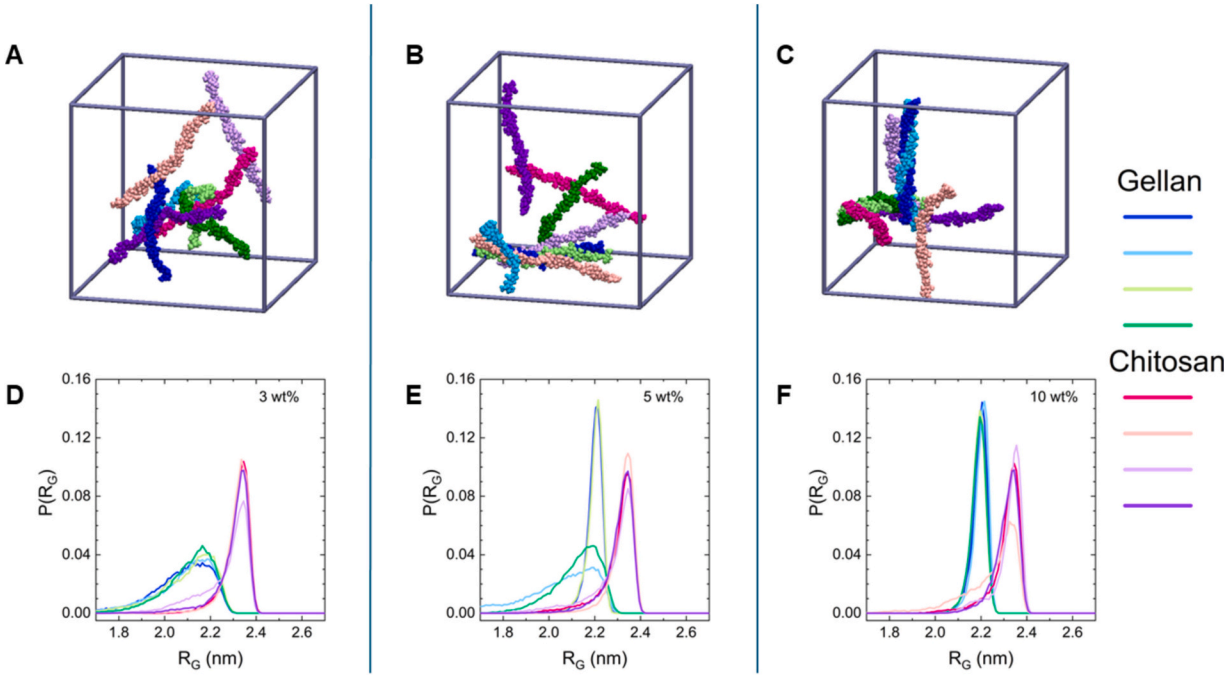

Fig. 7. Representative snapshots from all-atom MD simulations at 298 K of a suspension of polysaccharide chains with a gellan:chitosan ratio of 0.5:0.5 at concentration of (A) 3, (B) 5, and (C) 10 wt%. Ions and water molecules are omitted for clarity. Distribution of the radius of gyration ($P(R_G)$) of each polysaccharide chain at 298 K calculated for a suspension of polysaccharide chains with a gellan:chitosan ratio $R = 0.5{:}0.5$ at concentration of (D) 3 wt%, (E) 5 wt%, and (F) 10 wt% over the last 200 ns of simulation data.

addition, Figs. 7B and C suggest that the association of pair of gellan chains occurs through the formation of double helix structures (blue and green chains), in analogy with what observed in previous studies of suspensions of gellan chains in water [7] and in DLS analysis (Fig. 2C).

To get information on the chain conformation in aqueous solution, the distribution of the radius of gyration of polysaccharide chains is then analyzed. Figs. 7D, E, F compare the results obtained for each chain in the different systems. For chitosan chains, in all systems, the distribution of the radius of gyration of the chains is narrow with a maximum located at 2.35 nm, and it is not affected by the polysaccharide concentration. These findings were further compared with those obtained for an independent simulation of pure chitosan chains in water at a polysaccharide concentration of 5 wt%, as reported in Fig. S4. In the absence of gellan chains, the distribution of radius of gyration is again narrow with a single maximum at 2.35 nm, suggesting that the presence of gellan does not significantly affect chitosan conformation.

Differently, for gellan chains changes in chain conformation were detected. Fig. 7D shows that at the lowest polysaccharide concentration, at which the system aggregation is less marked, the distribution of radius of gyration of gellan chains is broad. Conversely, Figs. 7E and F reveal that when aggregation is more extensive, gellan chains assume a narrow distribution of the radius of gyration with a maximum located at 2.2 nm, which is indicative of the formation of double helix structures, as demonstrated in the study of pure gellan suspensions in water [7]. Indeed, in Ref. [7] it is demonstrated that the conformational transition of gellan chains observed in Fig. 7E and F, which leads to more rigid and elongated conformation, corresponds to the formation of double helix structures. This is also highlighted in Figs. 7B and C, where the gellan chains (shown in blue and green), that in Fig. 7E and F are characterized by a narrow distribution of the radius of gyration with a maximum located at 2.2 nm, clearly form double helices.

The self-assembly process was further examined by analyzing the hydrogen bonding interactions occurring in solution. First, the hydration properties were characterized, as illustrated in Fig. 8A which shows the average number of hydrogen bonds formed between the polysaccharide chains and water. It is interesting to note that, at the lowest polysaccharide concentration, gellan chains exhibit a higher degree of hydration. However, when the polysaccharide concentration is increased gellan chains tend to dehydrate, whereas chitosan hydration features are weakly affected by the concentration. Similarly, by monitoring the polysaccharide-polysaccharide hydrogen bonds, as shown in Fig. 8B, gellan chains are able to form a higher number of hydrogen bonds, which increases with the polysaccharide concentration. Instead, the number of hydrogen bonds formed by the chitosan chains is almost independent of the concentration. Nonetheless, mixed chitosan-gellan hydrogen bonds are favored at the higher concentrations and association degree.

Hereafter the focus is on the system with polysaccharide concentration of 10 wt%, in which the most extended aggregation is detected, to investigate in detail the mechanism of gellan-chitosan complexation. Fig. 8C compares the radial distribution functions (RDF) calculated for specific atoms in the system and averaged over the last 200 ns of simulation trajectory. Carbon atom of the carboxylate group and the nitrogen atom of the amine group were used as probe of gellan (G) and chitosan (C) behavior, respectively, and homo and hetero interactions were monitored, as well as interactions with the oxygen atom of water (W), sodium (Na) and chloride (CL) counterions. RDF of G-G atoms is characterized by two peaks located at about 8 Å and 12 Å, which are indicative of a double helix structure, similarly to what observed in gellan chain suspensions [7]. Moreover, less intense peaks of G-Na and G-W at lower distances were observed, thus indicating sodium counterions and water molecules directly interacting with the carboxylate moiety of gellan. For chitosan, the RDF of C-C is characterized by two peaks placed at about 7.5 Å and 11 Å, arising from the nearest-neighbor and 1–3 interactions of nitrogen atoms belonging to an individual chitosan chain. Thus, no self-assembly of chitosan chains is revealed in the polysaccharide suspension in water. In addition, at shorter distances higher peaks for RDF of C-CL and C-W are detected, with respect to RDF G-Na and G-W, describing a more hydrated system. Nonetheless, the RDF of C-G is characterized by a peak placed at about 3.4 Å, which suggests the occurrence of electrostatic interactions between gellan and chitosan chains.

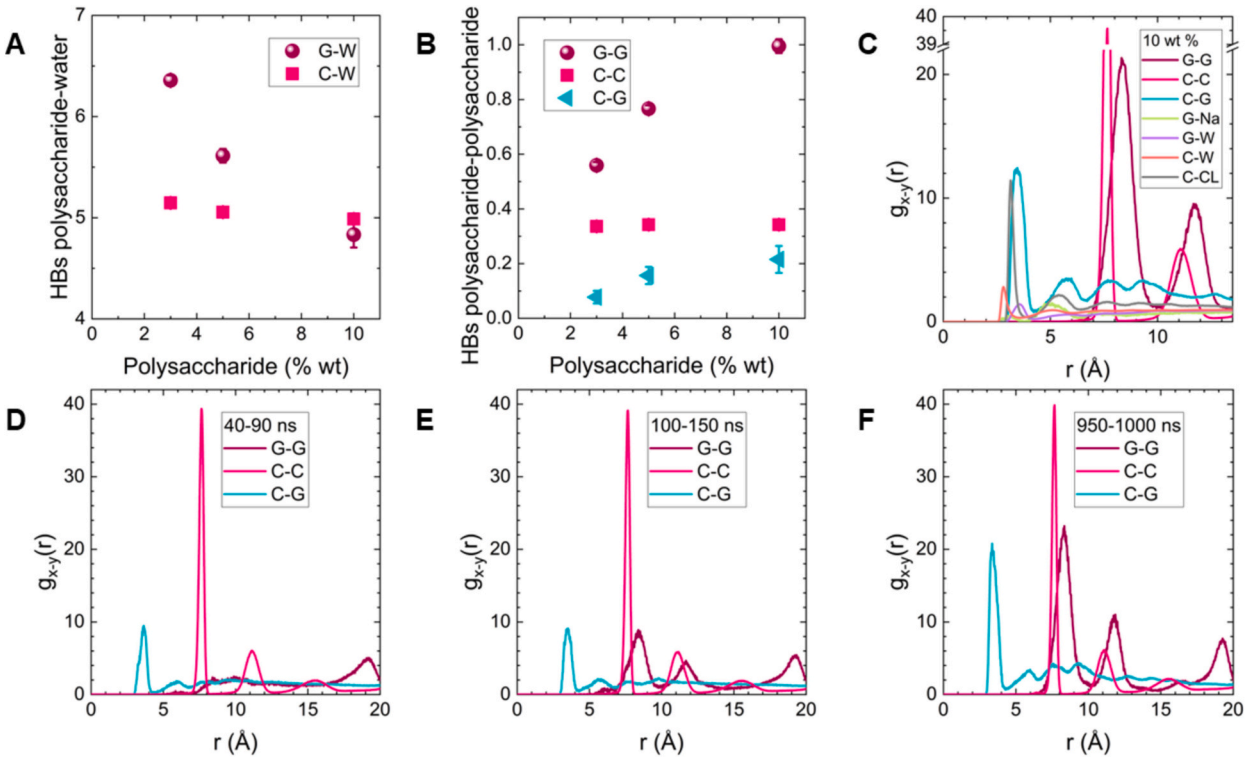

Fig. 8. Average number of (A) polysaccharide-water, and (B) polysaccharide-polysaccharide hydrogen bonds normalized to the number of monosaccharides and averaged over the last 200 ns of simulation as a function of the total polysaccharide concentration. Gellan-water (G-W), chitosan-water (C-W), gellan-gellan (G-G), chitosan-chitosan (C-C), and chitosan-gellan (C-G) hydrogen bonds are shown with red spheres, magenta squares, red spheres, magenta squares, and cyan triangles, respectively. (C) Radial distribution functions (RDF) calculated at 298 K for the gellan-chitosan suspension at a polysaccharide concentration of 10 wt%. RDF calculated for gellan carboxylate carbon (G-G), chitosan amine nitrogen (C-C), chitosan amine nitrogen and gellan carboxylate carbon (C-G), gellan carboxylate carbon and sodium counterion (G-Na), gellan carboxylate carbon and water oxygen (G-W), chitosan amine nitrogen and water oxygen (C-W), chitosan amine nitrogen and chloride counterion (C-CL), are shown in red, magenta, cyan, green, purple, orange, and gray, respectively. RDF calculated at 298 K for the gellan-chitosan suspension at a polysaccharide concentration of 10 wt% for three different simulation time intervals: (D) from 40 ns to 90 ns, (E) from 100 ns to 150 ns, and (F) from 950 ns to 1000 ns. RDF calculated for gellan carboxylate carbon (G-G), chitosan amine nitrogen (C-C), chitosan amine nitrogen and gellan carboxylate carbon (C-G), are shown in red, magenta, and cyan, respectively.

To distinguish and analyze independently the different steps of the microscopic mechanism of gellan-chitosan complexation, the system with polysaccharide concentration of 10 wt% is studied as a function of time. Figs. 8D, E, F report the RDF calculated for the carbon atom of the carboxylate group of gellan (G-G), the nitrogen atom of the amine group of chitosan (C-C) and the mixture of the two types of atoms (C-G) averaged over 50 ns of simulations trajectory, during which the polysaccharide suspension is characterized by the presence of either 0 (D), or 1 (E), or 2 (F) gellan double helix structures. RDF of C-C is weakly affected by the stage of the complexation process, as observed, appearing very similar in the three analyzed time intervals. On the other hand, when moving from a state with no double helix (Fig. 8D) to a state with one double helix (Fig. 8E), the RDF of G-G shows the appearance of two peaks located at about 8 Å and 12 Å, which is associated to the double helix formation. This is also confirmed in Fig. 8F, where the presence of two double helix structures further increases the intensity of these two peaks. Finally, the RDFs of C-G calculated in the systems without or with only one gellan double helix are similar. However, a significant increase of the peak of RDF of C-G located at about 3.4 Å is detected when two gellan double helices are formed, indicating the occurrence of strong electrostatic interactions between gellan carboxylate and chitosan amine groups (as suggested by experimental results).

Based on these findings, the RDF of C-G is used to probe the formation mechanism of gellan-chitosan PECs, and to directly compare the systems at different concentrations by multiplying the RDF by the particle density (ρ), as reported in Fig. 9A. It was found that the RDFs of C-G calculated in a trajectory interval where no gellan double helixes are formed, at concentration of 3 and 5 wt%, are very similar to each other, being characterized by essentially a low intensity first peak. Furthermore, when RDFs of C-G are calculated in a time interval where one gellan double helix is present in solution, at concentration of 5 and 10 wt %, the two curves are very similar to each other, with the first peak increasing in intensity in both systems and moving towards shorter distances. Finally, for the RDF of C-G calculated where two gellan double helices are formed, at a concentration of 10 wt%, the intensity of the first peak has an even stronger increase, again moving to shorter distances. Furthermore, the RDF of C-G displays a clear progressive structuring with the onset of one and two double helices, as evidenced by the significant increase of the number and intensity of additional peaks, up to the fourth one. These results clearly reveal that gellan and chitosan assemble into PECs with a highly ordered arrangement of the two polymers with respect to each other. Altogether, the numerical findings clarify the mechanism of gellan-chitosan complexation, revealing that it takes place in multiple steps: at first, through the association of gellan chains into double helix structures, which then drives the further association of chitosan chains thanks to the formation of ionic pairs and hydrogen bonding interactions. In Fig. 10 a schematic illustration of the mechanism of PECs formation is reported, to visualize how gellan and chitosan chains interact.

4. Conclusions

This study provides a thorough characterization of gellan-chitosan PECs, offering a molecular understanding of the complexation

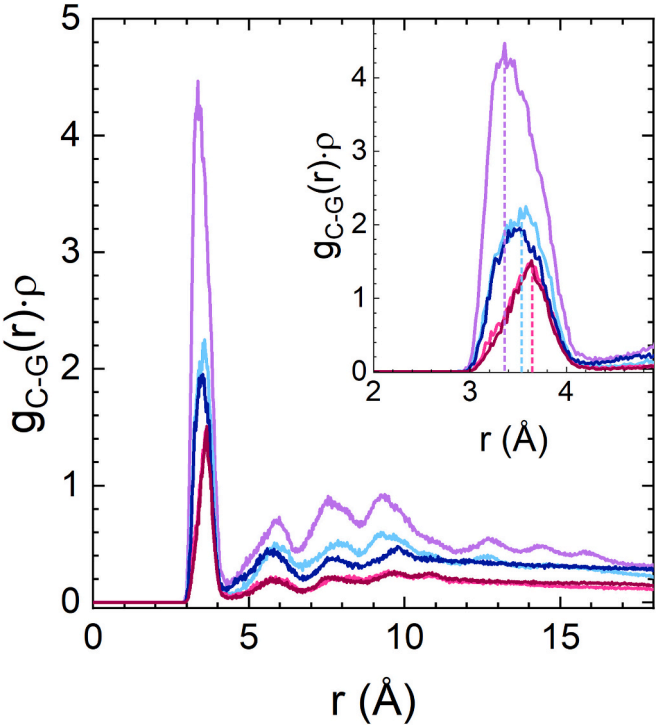

Fig. 9. (A) Comparison between RDFs multiplied by the particle density (ρ) calculated for chitosan amine nitrogen and gellan carboxylate carbon (C-G) averaged over 50 ns at a concentration of 3 wt% (pink) and 5 wt% (red) in time intervals where no gellan double helix is observed, at a concentration of 5 wt% (light blue) and 10 wt% (blue) in time intervals where1 gellan double helix is observed, and at a concentration of 10 wt% (purple) in time intervals where 2 gellan double helixes are observed. The inset highlights the first peak. Vertical lines indicate first peak positions.

mechanism based on a combination of experiments and atomistic molecular dynamics simulations. The formation of gellan-chitosan complexes is probed by using DLS and ζ-potential measurements, showing that electrostatic complexation between gellan and chitosan leads to the formation of heterogeneous nanoaggregates, characterized by a positive charge and good colloidal stability. ATR-FTIR measurements further confirm the complexes formation, while the macroscopic morphology of gellan-chitosan PECs is revealed by means of AFM investigation. The conformation of the polysaccharides in solution is also characterized by using CD spectroscopy, showing that gellan chains are preferentially organized in double helix structures, regardless of the presence of chitosan, and that the complexation with chitosan does not significantly affect their conformational features.

A detailed molecular understanding of the complexation mechanism is reached by using atomistic molecular dynamics simulations. These results reveal that the mechanism of formation of gellan-chitosan PECs involves a two-step process: first, gellan chains self-assemble into double helix structures, and then the association of chitosan chains occurs by forming electrostatic and hydrogen bonding interactions. The PECs are characterized at the different stages of this complex process, highlighting the increased structural order within the complexes once aggregation takes place. Simulation results further suggest that the features of each polysaccharide are not significantly altered by the complexation process. These results are in agreement with the formulated starting hypothesis, supporting the potential of the investigated chitosan/gellan PECs in the bio-technological field. For instance, it has been recently shown that microgels based on gellan are promising cleaning agents for art restoration [15] and the incorporation of chitosan could improve their efficacy by adding antibacterial properties. Overall, these insights will promote further research on polysaccharide aggregation mechanisms and expand the applications of the PECs in diverse fields.

CRediT authorship contribution statement

Leonardo Severini: Conceptualization, Methodology, Investigation, Formal analysis, Data curation, Writing – original draft, Writing - review & editing. **Letizia Tavagnacco:** Conceptualization, Software, Methodology, Investigation, Formal analysis, Data curation, Writing – original draft, Writing - review & editing. **Simona Sennato:** Conceptualization, Supervision, Investigation, Methodology, Data Curation, Writing – original draft, Writing - review & editing. **Erika Celi:** Validation, Investigation, Writing - review & editing. **Ester Chiessi:** Conceptualization, Supervision, Investigation, Methodology, Writing – original draft, Writing - review & editing. **Claudia Mazzuca:** Conceptualization, Supervision, Investigation, Methodology, Data Curation, Writing – original draft, Writing - review & editing. **Emanuela Zaccarelli:** Conceptualization, Supervision, Investigation, Methodology, Resources, Project Administration, Funding acquisition, Writing – original draft, Writing - review & editing.

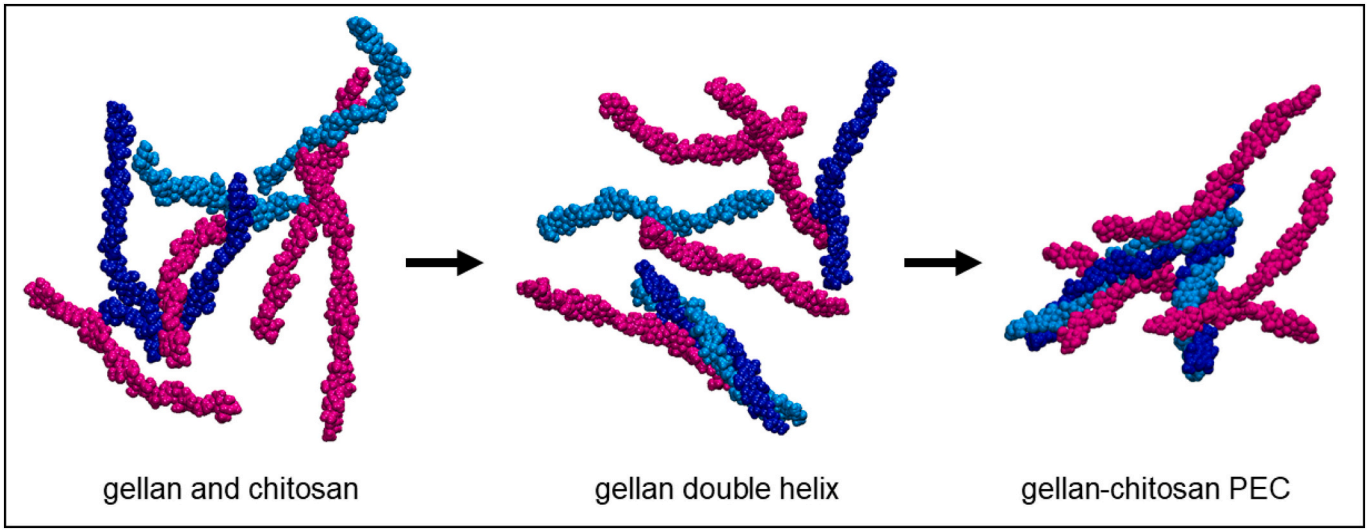

Fig. 10. Schematic illustration of the formation of gellan-chitosan polyelectrolyte complexes. Gellan chains are shown in blue and cyan to highlight the double helix structure, while chitosan chains are displayed in pink.

Declaration of competing interest

The authors declare no competing financial interest.

Acknowledgements

Financial support from ERC POC project MICROTECH (grant agreement no. 101066434) is gratefully acknowledged. LT and EZ also acknowledge financial support from ICSC – Centro Nazionale di Ricerca in High Performance Computing, Big Data and Quantum Computing, funded by European Union – NextGenerationEU – PNRR, Missione 4 Componente 2 Investimento 1.4. CINECA-ISCRA is acknowledged for HPC resources. The authors acknowledge the Physics Department of Sapienza University of Rome for providing access to SNN-Lab of the Research Center on Nanotechnology Applied to Engineering of Sapienza University (CNIS) for AFM measurements.

Appendix A. Supplementary data

Supplementary data to this article can be found online at https://doi.org/10.1016/j.ijbiomac.2024.139098.

Data availability

Data for this article are available on the online repository Zenodo (https://doi.org/10.5281/zenodo.14558119).

References

[1] J.J. McManus, P. Charbonneau, E. Zaccarelli, N. Asherie, The physics of protein self-assembly, Curr. Opin. Colloid Interface Sci. 22 (2016) 73–79, https://doi.org/10.1016/j.cocis.2016.02.011.
[2] R. Stern, M.J. Jedrzejas, Carbohydrate polymers at the Center of Life's origins: the importance of molecular processivity, Chem. Rev. 108 (2008) 5061–5085, https://doi.org/10.1021/cr078240l.
[3] R. Har-El, M.L. Tanzer, Extracellular matrix 3: evolution of the extracellular matrix in invertebrates, FASEB J. 7 (1993) 1115–1123, https://doi.org/10.1096/fasebj.7.12.8375610.
[4] T.W. Bell, H. Jousselin, Self-assembly of a double-helical complex of sodium, Nature 367 (1994) 441–444, https://doi.org/10.1038/367441a0.
[5] G.M.L. Messina, G. Bocchinfuso, N. Giamblanco, C. Mazzuca, A. Palleschi, G. Marletta, Orienting proteins by nanostructured surfaces: evidence of a curvature-driven geometrical resonance, Nanoscale 10 (2018) 7544–7555, https://doi.org/10.1039/C8NR00037A.
[6] G.M.L. Messina, B. Di Napoli, M. De Zotti, C. Mazzuca, F. Formaggio, A. Palleschi, G. Marletta, Molecular sponge: pH-driven reversible squeezing of stimuli-sensitive peptide monolayers, Langmuir 35 (2019) 4813–4824, https://doi.org/10.1021/acs.langmuir.8b03895.
[7] L. Tavagnacco, E. Chiessi, L. Severini, S. Franco, E. Buratti, A. Capocefalo, F. Brasili, A. Mosca Conte, M. Missori, R. Angelini, S. Sennato, C. Mazzuca, E. Zaccarelli, Molecular origin of the two-step mechanism of gellan aggregation, Sci. Adv. 9 (2023) eadg4392, https://doi.org/10.1126/sciadv.adg4392.
[8] G. Verma, P.A. Hassan, Self assembled materials: design strategies and drug delivery perspectives, Phys. Chem. Chem. Phys. 15 (2013) 17016, https://doi.org/10.1039/c3cp51207j.
[9] L. Severini, K.J. De France, D. Sivaraman, N. Kummer, G. Nyström, Biohybrid nanocellulose–lysozyme amyloid aerogels via electrostatic complexation, ACS Omega 7 (2022) 578–586, https://doi.org/10.1021/acsomega.1c05069.
[10] K.A.M. Amin, M. In Het Panhuis, Polyelectrolyte complex materials from chitosan and gellan gum, Carbohydr. Polym. 86 (2011) 352–358, https://doi.org/10.1016/j.carbpol.2011.04.035.
[11] L. Wang, E. Khor, A. Wee, L.Y. Lim, Chitosan-alginate PEC membrane as a wound dressing: assessment of incisional wound healing, J. Biomed. Mater. Res. 63 (2002) 610–618, https://doi.org/10.1002/jbm.10382.
[12] D. Wu, L. Zhu, Y. Li, X. Zhang, S. Xu, G. Yang, T. Delair, Chitosan-based colloidal polyelectrolyte complexes for drug delivery: a review, Carbohydr. Polym. 238 (2020) 116126, https://doi.org/10.1016/j.carbpol.2020.116126.
[13] A.S. Weingarten, R.V. Kazantsev, L.C. Palmer, M. McClendon, A.R. Koltonow, A.P. S. Samuel, D.J. Kiebala, M.R. Wasielewski, S.I. Stupp, Self-assembling hydrogel scaffolds for photocatalytic hydrogen production, Nat. Chem. 6 (2014) 964–970, https://doi.org/10.1038/nchem.2075.
[14] H. Li, L. Severini, M. Titubante, D. Gong, L. Micheli, C. Mazzuca, Y. Gong, Gellan gum hydrogel as an aqueous treatment method for *Xuan* paper, Restaur. Int. J. Preserv. Libr. Arch. Mater. 42 (2021) 37–54, https://doi.org/10.1515/res-2020-0010.
[15] B. Di Napoli, S. Franco, L. Severini, M. Tumiati, E. Buratti, M. Titubante, V. Nigro, N. Gnan, L. Micheli, B. Ruzicka, C. Mazzuca, R. Angelini, M. Missori, E. Zaccarelli, Gellan gum microgels as effective agents for a rapid cleaning of paper, ACS Appl. Polym. Mater. 2 (2020) 2791–2801, https://doi.org/10.1021/acsapm.0c00342.
[16] A.V. Ilina, V.P. Varlamov, Chitosan-based polyelectrolyte complexes: A review, Appl. Biochem. Microbiol. 41 (2005) 5–11, https://doi.org/10.1007/s10438-005-0002-z.
[17] L.M. Bravo-Anaya, J.F.A. Soltero, M. Rinaudo, DNA/chitosan electrostatic complex, Int. J. Biol. Macromol. 88 (2016) 345–353, https://doi.org/10.1016/j.ijbiomac.2016.03.035.
[18] X. Zhang, D. Liu, T.Z. Jin, W. Chen, Q. He, Z. Zou, H. Zhao, X. Ye, M. Guo, Preparation and characterization of gellan gum-chitosan polyelectrolyte complex films with the incorporation of thyme essential oil nanoemulsion, Food Hydrocoll. 114 (2021) 106570, https://doi.org/10.1016/j.foodhyd.2020.106570.
[19] V.D. Prajapati, G.K. Jani, B.S. Zala, T.A. Khutliwala, An insight into the emerging exopolysaccharide gellan gum as a novel polymer, Carbohydr. Polym. 93 (2013) 670–678, https://doi.org/10.1016/j.carbpol.2013.01.030.
[20] E.R. Morris, K. Nishinari, M. Rinaudo, Gelation of gellan – A review, Food Hydrocoll. 28 (2012) 373–411, https://doi.org/10.1016/j.foodhyd.2012.01.004.
[21] C.S.F. Picone, R.L. Cunha, Influence of pH on formation and properties of gellan gels, Carbohydr. Polym. 84 (2011) 662–668, https://doi.org/10.1016/j.carbpol.2010.12.045.
[22] M.A. Ibrahim, M.H. Alhalafi, E.-A.M. Emam, H. Ibrahim, R.M. Mosaad, A review of chitosan and chitosan nanofiber: preparation, characterization, and its potential applications, Polymers 15 (2023) 2820, https://doi.org/10.3390/polym15132820.
[23] W.M. Bruck, J. Slater, B. Carney, Chitin, Chitosan, Oligosaccharides and Their Derivatives, 2010.
[24] H. Honarkar, M. Barikani, Applications of biopolymers I: chitosan, Monatshefte Für Chem. - Chem. Mon. 140 (2009) 1403–1420, https://doi.org/10.1007/s00706-009-0197-4.
[25] S.B. da Silva, D. de Souza, L.D. Lacerda, Food applications of chitosan and its derivatives, in: L.A.M. Broek, C.G. Boeriu (Eds.), Chitin Chitosan, 1st ed, Wiley, 2019, pp. 315–347, https://doi.org/10.1002/9781119450467.ch13.
[26] C. Thambiliyagodage, M. Jayanetti, A. Mendis, G. Ekanayake, H. Liyanaarachchi, S. Vigneswaran, Recent advances in chitosan-based applications—a review, Materials 16 (2023) 2073, https://doi.org/10.3390/ma16052073.
[27] L.R. Fonseca, T.P. Santos, A. Czaikoski, R.L. Cunha, Microfluidics-based production of chitosan-gellan nanocomplexes encapsulating caffeine, Food Res. Int. 151 (2022) 110885, https://doi.org/10.1016/j.foodres.2021.110885.
[28] M. Amaike, Y. Senoo, H. Yamamoto, Sphere, honeycomb, regularly spaced droplet and fiber structures of polyion complexes of chitosan and gellan, Macromol. Rapid Commun. 19 (1998) 287–289, doi:10.1002/(SICI)1521-3927(19980601)19:6<287::AID-MARC287>3.0.CO;2-X.
[29] L. Ribas Fonseca, T. Porto Santos, A. Czaikoski, R. Lopes Cunha, Modulating properties of polysaccharides nanocomplexes from enzymatic hydrolysis of chitosan, Food Res. Int. 137 (2020) 109642, https://doi.org/10.1016/j.foodres.2020.109642.
[30] D.L. Roman, V. Ostafe, A. Isvoran, Deeper inside the specificity of lysozyme when degrading chitosan. A structural bioinformatics study, J. Mol. Graph. Model. 100 (2020) 107676, https://doi.org/10.1016/j.jmgm.2020.107676.
[31] C.S.F. Picone, R.L. Cunha, Chitosan–gellan electrostatic complexes: influence of preparation conditions and surfactant presence, Carbohydr. Polym. 94 (2013) 695–703, https://doi.org/10.1016/j.carbpol.2013.01.092.
[32] A.C. de Oliveira, B.H. Vilsinski, E.G. Bonafé, J.P. Monteiro, M.J. Kipper, A. F. Martins, Chitosan content modulates durability and structural homogeneity of chitosan-gellan gum assemblies, Int. J. Biol. Macromol. 128 (2019) 114–123, https://doi.org/10.1016/j.ijbiomac.2019.01.110.
[33] G. Sworn, S. Kasapis, Effect of conformation and molecular weight of co-solute on the mechanical properties of gellan gum gels, Food Hydrocoll. 12 (1998) 283–290, https://doi.org/10.1016/S0268-005X(98)00016-2.
[34] L. Severini, L. Tavagnacco, R. Angelini, S. Franco, M. Bertoldo, M. Calosi, L. Micheli, S. Sennato, E. Chiessi, B. Ruzicka, M. Missori, C. Mazzuca, E. Zaccarelli, Methacrylated gellan gum hydrogel: a smart tool to face complex problems in the cleaning of paper materials, Cellulose 30 (2023) 10469–10485, https://doi.org/10.1007/s10570-023-05479-z.
[35] J. Weißpflog, D. Vehlow, M. Müller, B. Kohn, U. Scheler, S. Boye, S. Schwarz, Characterization of chitosan with different degree of deacetylation and equal viscosity in dissolved and solid state – insights by various complimentary methods, Int. J. Biol. Macromol. 171 (2021) 242–261, https://doi.org/10.1016/j.ijbiomac.2021.01.010.
[36] D.E. Koppel, Analysis of macromolecular polydispersity in intensity correlation spectroscopy: the method of Cumulants, J. Chem. Phys. 57 (1972) 4814–4820, https://doi.org/10.1063/1.1678153.
[37] C. Lawson, R. Hanson, Solving least squares problems, in: Soc. Ind. Appl. Math, Prentice Hall, Englewood Cliffs, 1974.
[38] W.W. Tscharnuter, Mobility measurements by phase analysis, Appl. Optics 40 (2001) 3995, https://doi.org/10.1364/AO.40.003995.
[39] M.J. Abraham, T. Murtola, R. Schulz, S. Páll, J.C. Smith, B. Hess, E. Lindahl, GROMACS: high performance molecular simulations through multi-level parallelism from laptops to supercomputers, SoftwareX 1–2 (2015) 19–25, https://doi.org/10.1016/j.softx.2015.06.001.
[40] S. Markidis, E. Laure (Eds.), Solving Software Challenges for Exascale: International Conference on Exascale Applications and Software, EASC 2014, Stockholm, Sweden, April 2-3, 2014, Revised Selected Papers, Springer International Publishing, Cham, 2015, https://doi.org/10.1007/978-3-319-15976-8.

[41] R. Chandrasekaran, R.P. Millane, S. Arnott, E.D.T. Atkins, The crystal structure of gellan, Carbohydr. Res. 175 (1988) 1–15, https://doi.org/10.1016/0008-6215(88)80151-4.
[42] T. Yui, K. Imada, K. Okuyama, Y. Obata, K. Suzuki, K. Ogawa, Molecular and crystal structure of the anhydrous form of chitosan, Macromolecule 27 (1994) 7601–7605.
[43] O. Guvench, S.N. Greene, G. Kamath, J.W. Brady, R.M. Venable, R.W. Pastor, A. D. Mackerell, Additive empirical force field for hexopyranose monosaccharides, J. Comput. Chem. 29 (2008) 2543–2564, https://doi.org/10.1002/jcc.21004.
[44] W.L. Jorgensen, J. Chandrasekhar, J.D. Madura, R.W. Impey, M.L. Klein, Comparison of simple potential functions for simulating liquid water, J. Chem. Phys. 79 (1983) 926–935, https://doi.org/10.1063/1.445869.
[45] M. Hosseinnejad, S.M. Jafari, Evaluation of different factors affecting antimicrobial properties of chitosan, Int. J. Biol. Macromol. 85 (2016) 467–475, https://doi.org/10.1016/j.ijbiomac.2016.01.022.
[46] L.H. Fasolin, C.S.F. Picone, R.C. Santana, R.L. Cunha, Production of hybrid gels from polysorbate and gellan gum, Food Res. Int. 54 (2013) 501–507, https://doi.org/10.1016/j.foodres.2013.07.026.
[47] C. Burgos-Díaz, M. Opazo-Navarrete, J.L. Palacios, T. Barahona, Y. Mosi-Roa, F. Anguita-Barrales, M. Bustamante, Synthesis of new chitosan from an endemic Chilean crayfish exoskeleton (Parastacus Pugnax): physicochemical and biological properties, Polymers 13 (2021) 2304, https://doi.org/10.3390/polym13142304.
[48] S. de Jong, F. van de Velde, Charge density of polysaccharide controls microstructure and large deformation properties of mixed gels, Food Hydrocoll. 21 (2007) 1172–1187, https://doi.org/10.1016/j.foodhyd.2006.09.004.
[49] J.H. Hamman, Chitosan based polyelectrolyte complexes as potential carrier materials in drug delivery systems, Mar. Drugs 8 (2010) 1305–1322, https://doi.org/10.3390/md8041305.
[50] F. Amaduzzi, F. Bomboi, A. Bonincontro, F. Bordi, S. Casciardi, L. Chronopoulou, M. Diociaiuti, F. Mura, C. Palocci, S. Sennato, Chitosan–DNA complexes: charge inversion and DNA condensation, Colloids Surf. B Biointerfaces 114 (2014) 1–10, https://doi.org/10.1016/j.colsurfb.2013.09.029.
[51] G. Maurstad, S. Danielsen, B.T. Stokke, The influence of charge density of chitosan in the compaction of the Polyanions DNA and xanthan, Biomacromolecules 8 (2007) 1124–1130, https://doi.org/10.1021/bm0610119.
[52] I.V. Blagodatskikh, E.A. Bezrodnykh, S.S. Abramchuk, A.V. Muranov, O. V. Sinitsyna, A.R. Khokhlov, V.E. Tikhonov, Short chain chitosan solutions: self-assembly and aggregates disruption effects, J. Polym. Res. 20 (2013) 73, https://doi.org/10.1007/s10965-013-0073-0.
[53] B.H. Morrow, G.F. Payne, J. Shen, pH-responsive self-assembly of polysaccharide through a rugged energy landscape, J. Am. Chem. Soc. 137 (2015) 13024–13030, https://doi.org/10.1021/jacs.5b07761.
[54] M. Rinaudo, Chitin and chitosan: properties and applications, Prog. Polym. Sci. 31 (2006) 603–632, https://doi.org/10.1016/j.progpolymsci.2006.06.001.
[55] A. Kong, Y. Ji, H. Ma, Y. Song, B. He, J. Li, A novel route for the removal of Cu(II) and Ni(II) ions via homogeneous adsorption by chitosan solution, J. Clean. Prod. 192 (2018) 801–808, https://doi.org/10.1016/j.jclepro.2018.04.271.
[56] L. Wang, J. Wu, Y. Guo, C. Gong, Y. Song, Topographic characterization of the self-assembled nanostructures of chitosan on mica surface by atomic force microscopy, Appl. Surf. Sci. 353 (2015) 757–763, https://doi.org/10.1016/j.apsusc.2015.06.193.
[57] M.N.V. Ravi Kumar, A review of chitin and chitosan applications, React. Funct. Polym. 46 (2000) 1–27, https://doi.org/10.1016/S1381-5148(00)00038-9.
[58] M. Diener, J. Adamcik, J. Bergfreund, S. Catalini, P. Fischer, R. Mezzenga, Rigid, fibrillar quaternary structures induced by divalent ions in a carboxylated linear polysaccharide, ACS Macro Lett. 9 (2020) 115–121, https://doi.org/10.1021/acsmacrolett.9b00824.
[59] Q. Guo, S.W. Cui, Q. Wang, X. Hu, Q. Guo, J. Kang, R. Yada, Extraction, fractionation and physicochemical characterization of water-soluble polysaccharides from Artemisia sphaerocephala Krasch seed, Carbohydr. Polym. 86 (2011) 831–836, https://doi.org/10.1016/j.carbpol.2011.05.034.
[60] J. Kang, S.W. Cui, J. Chen, G.O. Phillips, Y. Wu, Q. Wang, New studies on gum ghatti (Anogeissus latifolia) part I. Fractionation, chemical and physical characterization of the gum, Food Hydrocoll. 25 (2011) 1984–1990, https://doi.org/10.1016/j.foodhyd.2010.12.011.
[61] D.R. Pereira, J. Silva-Correia, S.G. Caridade, J.T. Oliveira, R.A. Sousa, A.J. Salgado, J.M. Oliveira, J.F. Mano, N. Sousa, R.L. Reis, Development of Gellan gum-based microparticles/hydrogel matrices for application in the intervertebral disc regeneration, Tissue Eng. Part C Methods 17 (2011) 961–972, https://doi.org/10.1089/ten.tec.2011.0115.
[62] J. Singh, P.K. Dutta, Preparation, circular dichroism induced helical conformation and optical property of chitosan acid salt complexes for biomedical applications, Int. J. Biol. Macromol. 45 (2009) 384–392, https://doi.org/10.1016/j.ijbiomac.2009.07.004.
[63] J. Horinaka, K. Kani, Y. Hori, S. Maeda, Effect of pH on the conformation of gellan chains in aqueous systems, Biophys. Chem. 111 (2004) 223–227, https://doi.org/10.1016/j.bpc.2004.06.003.
[64] Y. Tanaka, M. Sakurai, K. Nakamura, Ultrasonic velocity and circular dichroism in aqueous gellan solutions, Food Hydrocoll. 10 (1996) 133–136, https://doi.org/10.1016/S0268-005X(96)80026-9.
[65] A. Domard, pH and c.d. measurements on a fully deacetylated chitosan: application to CuII—polymer interactions, Int. J. Biol. Macromol. 9 (1987) 98–104, https://doi.org/10.1016/0141-8130(87)90033-X.